THE JOURNAL OF BIOLOGICAL CHEMISTRY
Vol. 278, No. 20, Issue of May 16, pp. 18401–18407, 2003

Printed in U.S.A.

Structural Basis of Fosmidomycin Action Revealed by the Complex with 2-*C*-Methyl-D-erythritol 4-phosphate Synthase (IspC)

IMPLICATIONS FOR THE CATALYTIC MECHANISM AND ANTI-MALARIA DRUG DEVELOPMENT*

Received for publication, January 29, 2003, and in revised form, March 4, 2003
Published, JBC Papers in Press, March 5, 2003, DOI 10.1074/jbc.M300993200

Stefan Steinbacher‡§, Johannes Kaiser¶, Wolfgang Eisenreich¶, Robert Huber‡, Adelbert Bacher¶, and Felix Rohdich¶

From the ‡Max-Planck-Institut für Biochemie, Abteilung für Strukturforschung, Am Klopferspitz 18a, D-82152 Martinsried, Germany and the ¶Lehrstuhl für Organische Chemie und Biochemie, Technische Universität München, Lichtenbergstrasse 4, D-85747 Garching, Germany

2-*C*-Methyl-D-erythritol 4-phosphate synthase (IspC) is the first enzyme committed to isoprenoid biosynthesis in the methylerythritol phosphate pathway, which represents an alternative route to the classical mevalonate pathway. As it is present in many pathogens and plants, but not in man, this pathway has attracted considerable interest as a target for novel antibiotics and herbicides. Fosmidomycin represents a specific high-affinity inhibitor of IspC. Very recently, its anti-malaria activity in man has been demonstrated in clinical trials. Here, we present the crystal structure of *Escherichia coli* IspC in complex with manganese and fosmidomycin at 2.5 Å resolution. The (*N*-formyl-*N*-hydroxy)amino group provides two oxygen ligands to manganese that is present in a distorted octahedral coordination, whereas the phosphonate group is anchored in a specific pocket by numerous hydrogen bonds. Both sites are connected by a spacer of three methylene groups. The substrate molecule, 1-D-deoxyxylulose 5-phosphate, can be superimposed onto fosmidomycin, explaining the stereochemical course of the reaction.

Malaria represents one of the most threatening diseases especially in developing countries with about 300 million cases every year, resulting in more than one million deaths per year (1). Although it had been believed that malaria will be eradicated shortly, the present experience is to the contrary because the disease is escalating even in countries with satisfactory medical services. This and the development of multi-resistant variants of other pathogenic organisms define the urgent need for novel chemotypes of antibiotics that expand the repertoire of the presently targeted biochemical pathways (2, 3). The availability of the genome sequence of *Plasmodium falciparum*, the causative agent of malaria, and especially the wealth of information on the biochemical pathways used by this organism have opened novel approaches for drug development (4, 5). Specifically, the mevalonate-independent "2-*C*-methyl-D-erythritol 4-phosphate (MEP)[1] pathway" (Fig. 1*a*), which leads to the universal isoprenoid precursors isopentenyl diphosphate (IPP) (Fig. 1*a*, *4*) and dimethylallyl diphosphate (DMAPP) (Fig. 1*a*, *5*) via 2-*C*-methyl-D-erythritol 4-phosphate (Fig. 1*a*, *2*) and (*E*)-1-hydroxy-2-methyl-but-2-enyl 4-diphosphate (Fig. 1*a*, *3*) has attracted considerable interest (6, 7). The existence of this pathway in certain eubacteria and plants has been demonstrated by pioneering studies of Rohmer *et al.* (8) and Arigoni and co-workers (9, 10) (reviewed in Refs. 11–13). Evidence has been accumulated for its presence in many pathogenic microorganisms including the malaria parasite *Plasmodium* spp. that harbor the MEP pathway in their apicoplast compartments (14). As the pathway is not present in man where IPP and DMAPP are exclusively synthesized via mevalonate (Fig. 1*a, 6*), all enzymes of the 2-*C*-methyl-D-erythritol 4-phosphate (MEP) pathway represent promising targets for the development of novel drugs.

The first compound unique to the mevalonate-independent MEP pathway (Fig. 1*a*, *2*) is synthesized from 1-D-deoxyxylulose 5-phosphate (Fig. 1*a*, *1*) by IspC (15) *via* intramolecular rearrangement of 1-D-deoxyxylulose 5-phosphate (Fig. 1*a*, *1*) (10, 16–18) followed by NADPH-dependent reduction of the aldehyde intermediate, 2-*C*-methyl-D-erythrose 4-phosphate (Fig. 1*b*, *8*). The aldehyde intermediate can be chemically synthesized and converted either into the substrate, 1-D-deoxyxylulose 5-phosphate, or the product, 2-*C*-methyl-D-erythritol 4-phosphate, by IspC and nicotinamide nucleotides depending on the reaction conditions, which demonstrates not only full reversibility of the reaction but also that 2-*C*-methyl-D-erythrose 4-phosphate is a true intermediate (19). The stereochemical course of the reaction has been studied by isotope-labeling experiments and analysis of the resulting compounds by NMR spectroscopy both *in vivo* (20) and *in vitro* (21, 22). The enzymatic properties of IspC from *Escherichia coli* have been studied in detail (19, 23, 24). The enzymes from *E. coli*, *Chlamydomonas*, *Arabidopsis thaliana*, and *P. falciparum*, are susceptible to inhibition by fosmidomycin (Fig. 1*c*, *9*) (6, 23, 25,

* The costs of publication of this article were defrayed in part by the payment of page charges. This article must therefore be hereby marked "*advertisement*" in accordance with 18 U.S.C. Section 1734 solely to indicate this fact.

The atomic coordinates and structure factors (code 1ONN, 1ONO, and 1ONP) have been deposited in the Protein Data Bank, Research Collaboratory for Structural Bioinformatics, Rutgers University, New Brunswick, NJ (http://www.rcsb.org/).

§ Present address: Division of Chemistry and Chemical Engineering, Mail Code 114-96, California Inst. of Technology, Pasadena, CA 91125. To whom correspondence should be addressed. Tel.: 626-395-2662; Fax: 626-744-9524; E-mail: steinbac@caltech.edu.

[1] The abbreviations used are: MEP, 2-*C*-methyl-D-erythritol 4-phosphate; fosmidomycin, 3-(*N*-formyl-*N*-hydroxy)aminopropylphosphonic acid; FR-900098, 3-(N-acetyl-N-hydroxy)aminopropylphosphonic acid; IPP, isopentenyl diphosphate; DMAPP, dimethylallyl diphosphate; IspC, 2-*C*-Methyl-D-erythritol 4-phosphate synthase; DXP, 1-D-deoxyxylulose 5-phosphate; MN, crystals soaked with $MnCl_2$ added to the cryo solution; MNFOS, crystals soaked with $MnCl_2$ and fosmidomycin added to the cryo solution.

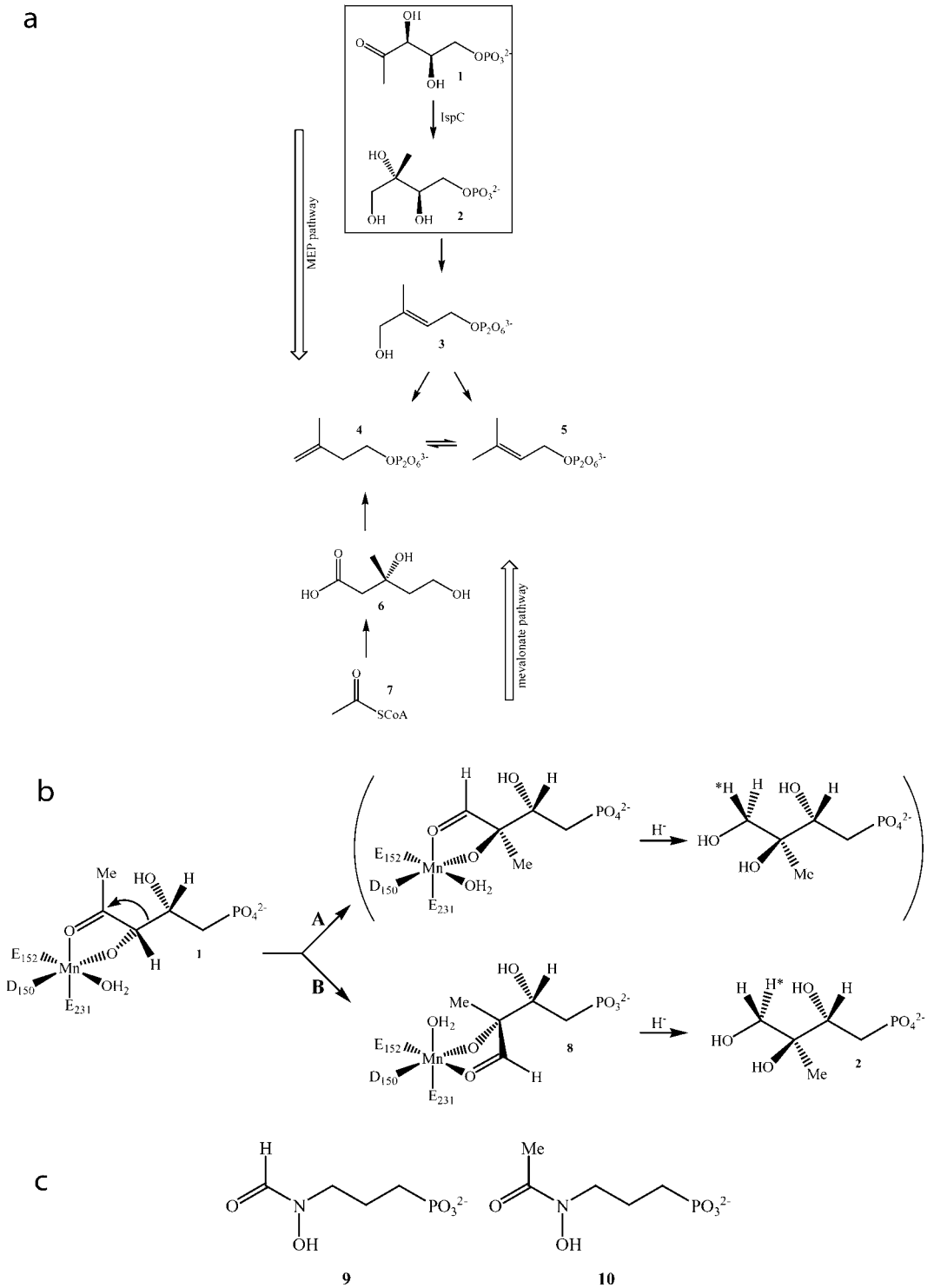

FIG. 1. *a*, methylerythritol phosphate and mevalonate pathway of isoprenoid biosynthesis. IPP (*4*) and DMAPP (*5*) are either synthesized from acetyl-CoA (*7*) via mevalonate (*6*) or from 1-deoxy-D-xylulose 5-phosphate (*1*) *via* 2-*C*-methyl-D-erythritol 4-phosphate (*2*) and (*E*)-1-hydroxy-2-methyl-but-2-enyl 4-diphosphate (*3*). *b*, stereochemical course of the reaction performed by IspC. 1-deoxy-D-xylulose 5-phosphate (*1*) is converted into 2-*C*-methyl-D-erythritol 4-phosphate (*4*) *via* the aldose intermediate 2-*C*-methyl-D-erythrose 4-phosphate (*8*) that is reduced by NADPH after isomerization. Route A for a fomidomycin-like binding of the intermediate *8* leads to the incorrect stereochemistry, whereas route B results in the correct stereochemistry. The migrating group (C-4) and the hydride from NADPH attack on opposite sites of C-2 and C-3, respectively. The *asterisk* indicates the hydride transferred from NADPH. *c*, chemical structures of the IspC inhibitors fosmidomycin (*9*) and FR-900098 (*10*).

26). Thus, fosmidomycin and its derivative, FR-900098 (Fig. 1*c*, *10*), have also been shown to cure mice infected by *Plasmodium vinckei* (6). Clinical trials showed that fosmidomycin can be used with a high rate of success for the treatment of malaria (7).

The three-dimensional structure of the *E. coli* enzyme without ligands and with NADPH and phosphate has been determined (27, 28). However, no structural information on substrate or inhibitor complexes is available. Here, we present the crystal structure of *E. coli* IspC in complex with the nanomolar inhibitor fosmidomycin at 2.5 Å resolution and discuss its implication for the reaction mechanism and the design of drugs.

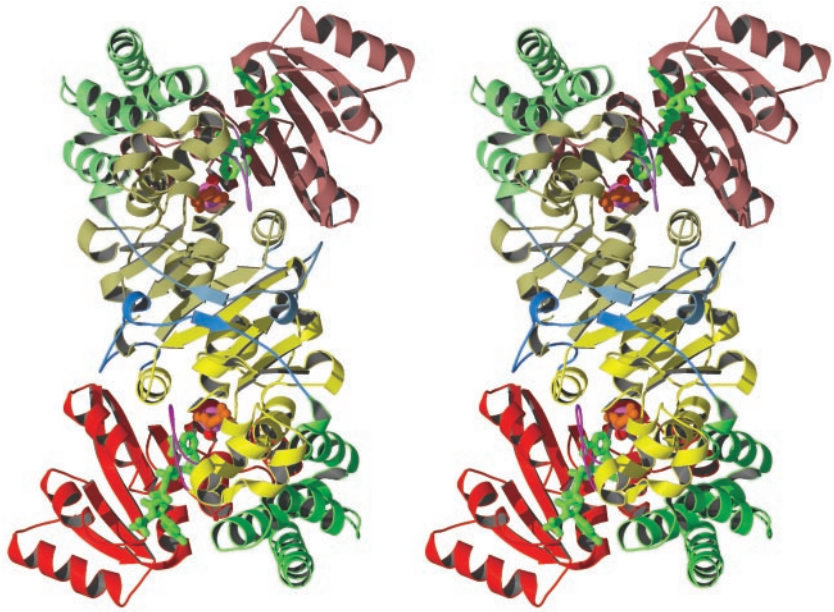

FIG. 2. **Ribbon diagram of the IspC dimer viewed along the dimer axis.** Each monomer can be divided into three domains. The N-terminal domain (*red*) binds NADPH (*light green ball-and-stick* model) and represents a classical dinucleotide binding fold. The central catalytic domain (*yellow*) binds the divalent metal (magnesium, manganese, or cobalt) and the substrate. Fosmidomycin is depicted as *orange ball-and-stick* model. It also harbors the flexible active site loop (*magenta*). A connecting stretch (*blue*) leads to a C-terminal α-helical domain that supports the catalytic domain.

MATERIALS AND METHODS

Expression, Purification, and Crystallization—The *ispC* gene of *E. coli* was cloned and overexpressed, and the corresponding gene product was purified as described previously (29). For crystallization, the protein was dialyzed against 100 mM Tris/HCl, pH 8.0, with 2 mM dithioerythritol and 0.02% (m/v) NaN_3 and concentrated to 10 mg/ml. 15 μl of the protein solution were mixed with 15 μl of the buffer solution containing 8% (w/v) polyethylene glycol (PEG) 4000 and 100 mM sodium acetate, 110 mM Hepes, 100 mM glycine, 100 mM guanidinium chloride, 10 mM EDTA, 12 mM dithiothreitol, pH 5.8, and equilibrated over 900 μl of the same buffer without EDTA in Linbro plates at 21 °C. The protein had a strong tendency to precipitate irreversibly. Diffraction quality crystals appeared rather irregularly after about 1 week and grew to a final size of about $0.45 \times 0.2 \times 0.2$ mm^3.

Structure Solution and Refinement—Data sets of the substrate-free crystals and the complexes were measured at 100 K using an Oxford cryo stream. Prior to flash freezing or soaking, the crystals were gradually transferred in about ten steps into a buffer solution containing the mother liquor without EDTA supplemented with 30% (v/v) polyethylene glycol 400 during a time period of about 30 min. For soaking, either 5 mM $MnCl_2$ (data set MN) or 5 mM $MnCl_2$ together with 2 mM fosmidomycin (data set MNFOS) were added to the cryo solution. Crystals were soaked for 2 h. Fosmidomycin was purchased from Molecular Probes (Eugene, Oregon).

X-ray diffraction data were collected on a MarResearch imaging plate detector mounted on a Rigaku rotating anode x-ray generator operating at 50 kV and 100 mA. Diffraction data were evaluated with the HKL suite (30) and CCP4 program suite (31). The crystal structure of the apo *E. coli* IspC (Protein Data Bank entry 1K5H) (27) of space group C222 (1) with three monomers in the asymmetric unit provided the starting set of coordinates. Model building was done with the program MAIN (32). The structures were refined with CNS (33) using a test set of 5% of the reflections for cross-validation. Starting *R*-factors after Patterson search with MOLREP (31) and rigid body refinement with crystallography NMR software were in the range of 43–47%. Models were refined by iterative rounds of model building, simulated annealing, least squares, and B-factor refinement. Finally, water molecules were picked with crystallography NMR software or manually. Non-crystallographic symmetry restraints were applied throughout the refinement. Initially the maximum likelihood target using amplitudes was applied, but in the final round the residual target was used because it was found to result in lower R_{free} values. The structures display good stereochemical parameters as estimated by the program PROCHECK (34). The Ramachandran plot (35) showed only 0.0% (apo), 1.3% (MN) or 0.8% (MNFOS) in the generously allowed region and 0.3% (apo) and 0.0% (MN and MNFOS) in the disallowed regions. Figures were prepared with BOBSCRIPT (36). The coordinates have been deposited with the Protein Data Bank under accession codes 1ONN, 1ONO, and 1ONP.

RESULTS AND DISCUSSION

Structure Solution—Recombinant 2-*C*-methyl-D-erythritol 4-phosphate synthase (EC 1.1.1.267) of *E. coli* has been crystallized in a monoclinic crystal form of space group P2(1) that is unrelated to that previously described (27, 28). The asymmetric unit contains a dimer that also represents the solution state of the enzyme (Fig. 2). The crystals showed unisotropic diffraction of x-ray to between 2.8 and 2.3 Å resolution and a rather high mosaicity of about ~1°. Based on the merging *R*-factor of the data and $I/\sigma(I)$ criteria for the outermost shell, useful data were included to a limiting resolution of 2.6 Å for the apo data set and 2.5 Å for the complex data sets with Mn^{2+} (MN) and Mn^{2+}/fosmidomycin (MNFOS), respectively (Table I). The known crystal structure of *E. coli* IspC (27) provided the starting model for the Patterson search. The resulting models were refined with non-crystallographic symmetry restraints until the crystallographic *R*-factors converged (Table I). The relatively high final R_{work} and R_{free} can be explained by the unisotropic diffraction and the high mosaicity. Nevertheless, the electron density was of high quality, and the Mn^{2+}/fosmidomycin moieties were excellently defined by simulated annealing omit maps (Fig. 3). Inclusion of non-crystallographic symmetry improved refinement behavior significantly, which indicates that both monomers are also rather similar with respect to their domain arrangement.

The model for the apo form contains residues 1–397 excluding the active site loop, which is completely disordered (residues Arg-208 to Gly-215). In the presence of Mn^{2+}/fosmidomycin, significant additional electron density is present for this loop that can be fitted as shown in Fig. 4. However, it appears that the catalytic loop remains partially disordered, especially for Ser-213 and Met-214, which are not defined by electron density, and it very likely adopts more than one conformation. Interestingly, Met-214 represents a strictly conserved residue. This can be explained if it is assumed that complete ordering of the catalytic loop requires the presence of both NADPH and the substrate 1-D-deoxyxylulose 5-phosphate.

Overall Structure—IspC forms an elongated homodimer of about 96×60 Å with a pronounced cleft-like structure in each monomer that is covered by a flexible active site loop (Fig. 2). Each monomer can be subdivided into basically three domains. The N-terminal domain (residues 1–149) is a member of the

TABLE I
Data collection and refinement statistics

Category	APO	MN	MNFOS
Data collection			
Space group P2(1) Cell constants (a, b, c in Å/β in °)	90.4, 53.4, 107.5/92.9	91.4, 52.3, 108.3/92.5	90.8, 52.3, 107.6/92.1
Limiting resolution (Å) (last shell)	2.6 (2.60–2.70)	2.5 (2.50–2.59)	2.5 (2.50–2.59)
Reflections	31,997	35,378	34,930
R_{merge}[a] (overall/last shell)	6.2 (40.5)	7.2 (35.6)	8.3 (41.7)
Redundancy	3.5	3.3	3.4
Completeness (%) (overall/last shell)	98.2 (98.4)	98.8 (99.7)	98.8 (98.5)
Refinement			
Resolution range (Å)	20–2.6	25–2.5	20–2.5
Reflections (working set)	29,882 (93.5%)	33,597 (93.8%)	33,163 (93.9%)
Reflections (test set)	1,557 (4.9%)	1,750 (4.9%)	1,725 (4.9%)
R_{cryst}(%)[b]	24.4	21.6	25.5
R_{free}(%)[c]	29.8	28.7	33.0
Non hydrogen protein atoms	5,912	5,912	6,048
Solvent molecules	316	197	143
B-factor (Å^2)			
Protein	58.0	61.8	69.3
Solvent	55.8	51.7	48.5
Manganese		49.6	64.7
Fos			77.7
Root mean square deviation			
Bond length [Å]	0.0105	0.0098	0.0108
Bond angle [°]	1.41	1.60	1.76

[a] $R_{merge} = \Sigma_{hkl} [\Sigma_i |I_i - <I>|)/\Sigma_i I]$.
[b] $R_{cryst} = \Sigma_{hkl} ||F_{obs}| - k|F_{calc}||/\Sigma_{hkl} |F_{obs}|$ for $hkl \subset$ working set.
[c] $R_{free} = \Sigma_{hkl} ||F_{obs}| - k|F_{calc}||/\Sigma_{hkl} |F_{obs}|$ for $hkl \subset$ test set.

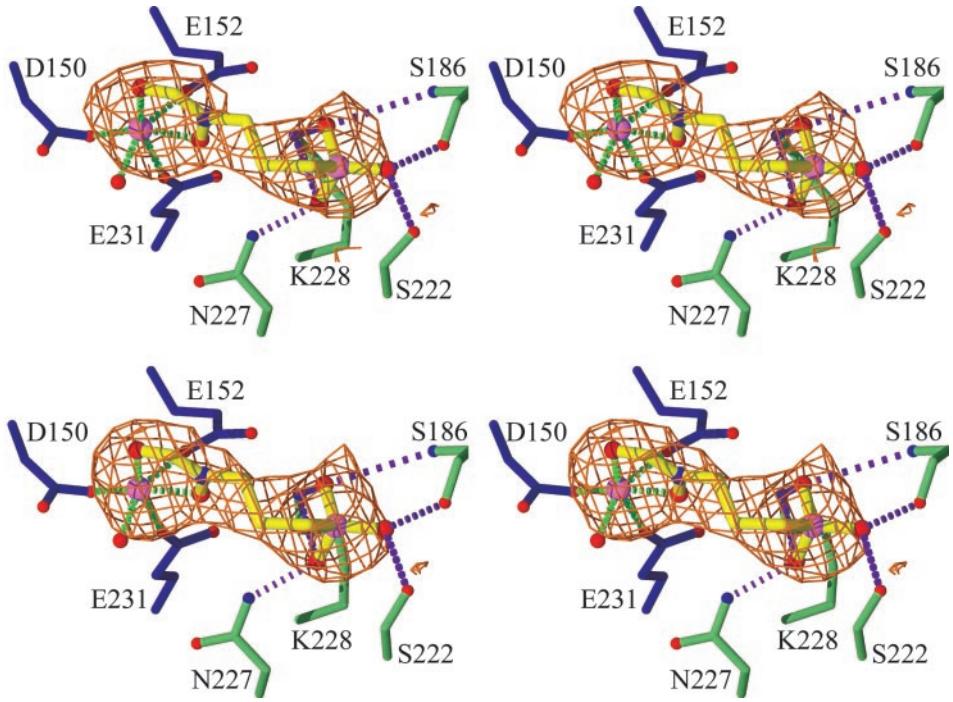

FIG. 3. **Simulated annealing $F_o - F_c$ omit map of bound manganese and fosmidomycin at 2.5 Å resolution for both asymmetric monomers.** The contour level is 3.5 σ.

classical dinucleotide binding fold and serves as an anchor for NADPH. A central catalytic domain (residues 150 to 285) harbors both the binding site for the divalent metal ion (Mg^{2+}, Mn^{2+}, or Co^{2+}), the phosphate binding site of the substrate, and the catalytic loop. The C-terminal all-α-helical domain (residues 312 to 398) is connected to the catalytic domain by a linker region that spans the entire monomer. The C-terminal domain appears to have a structural role in supporting the catalytic domain. The catalytic domain can even be subdivided into the part harboring the substrate binding site and that harboring the active site loop.

Binding of Manganese and Fosmidomycin and Implications for Anti-malaria Drug Development—IspC was crystallized in the absence of divalent metal ions, NADP(H) and substrate, or the inhibitor fosmidomycin. The NADPH binding site is blocked by the C terminus of a neighboring molecule in the crystal as found previously for an orthorhombic crystal form (27). The active site is well accessible in our crystals, and soaking with either Mn^{2+} or Mn^{2+} and fosmidomycin resulted in the corresponding electron densities (Fig. 3). Mn^{2+} is bound to a cluster of the carbonic acids, Asp-150, Glu-152, and Glu-231, as suggested previously (27). All residues form monodentate ligands, and a regular octahedral coordination sphere is completed by three water molecules. Upon the addition of fos-

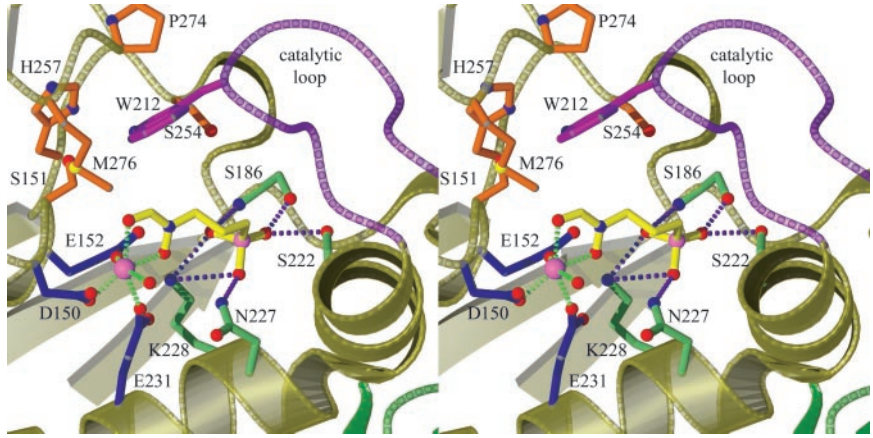

FIG. 4. **Active site geometry.** The divalent cation (Mn^{2+}) is bound to Asp-150, Glu-152, and Glu-231, which serve as monodentate ligands. The (*N*-formyl-*N*-hydroxy)amino head group of fosmidomycin (*yellow ball-and-stick* model) binds to Mn^{2+}; its phosphonate moiety is anchored by a H-bond network including Ser-186, Ser-222, Asn-227, and Lys-228. The catalytic loop (*magenta*) shows only weak electron density, which indicates an interaction of Trp-212 with a hydrophobic patch formed by His-257, Pro-274, and Met-276. A pronounced hydrophilic cavity behind fosmidomycin harbors Ser-151 and Ser-254.

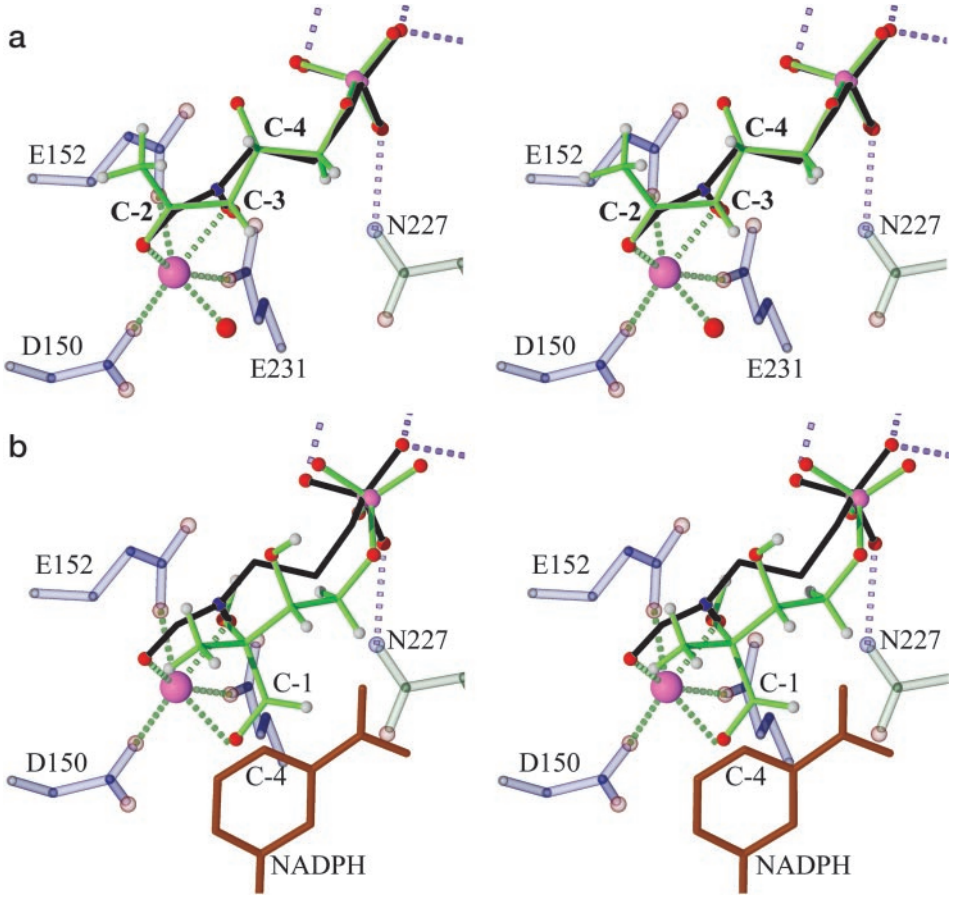

FIG. 5. **Modeled binding modes of the substrate and the aldehyde intermediate.** *a*, 1-D-deoxyxylulose 5-phosphate (in *green*) can be excellently superimposed onto fosmidomycin (in *black*). *b*, during the reaction, C-4 migrates to C-2. The nicotinamide moiety of NADPH was modeled according to Ref. 28 with only a slight adjustment, leaving its phosphate position unaltered. In this coordination, the stereochemistry of the hydride transfer to C-1 (former C-3 of the substrate) is compatible with the experimental data (compare Fig. 1*b*).

midomycin, two water molecules are replaced by its (*N*-formyl-*N*-hydroxy)amino head group. The geometry of the latter was modeled similar to that observed for the inhibitor 2-((formyl-(hydroxy)amino)methyl)-4-methylpentanoic acid complexed to zinc in the matrix metalloproteinase MMP9 (37). The *N*-formyl oxygen is found in the trans position to Glu-231, whereas the *N*-hydroxyl oxygen is located trans to Asp-150 (Fig. 4). The phosphonate moiety is anchored by numerous hydrogen bonds to Ser-186, Ser-222, Asn-227, and Lys-228. The conformation of the connecting linker that consists of three methylene groups appears clearly defined by electron density. Hydrophobic contacts of the latter do not seem to contribute to the high affinity of the inhibitor, as none is present with the rigid part of the binding site or apparently formed with the partially ordered catalytic loop. Trp-212 from the flexible catalytic loop is in direct vicinity to the bound inhibitor, although not well ordered. Replacement of His-257 by glutamine was found to have a drastic effect on the enzyme activity (38). The k_{cat}/K_m decreased 27,000-fold, and the K_m value for NADPH increased by approximately one order of magnitude, although it is quite far away from the NADPH binding site. The mutation of His-153 that is actually closer to the NADPH binding site does not have a comparable effect. This observation may be explained by an interaction between the His-257 site and the nicotinamide moiety that is mediated by the catalytic loop. It appears likely that His-257 and Trp-212 form a stacking interaction supported by

Pro-274 in the presence of NADPH that is a prerequisite for completely ordering the active site architecture.

Replacement of the formyl-hydrogen of fosmidomycin by a methyl group yields the inhibitor FR-900098 (Fig. 1*c*, *10*) (39) with increased affinity (6). This methyl group is predicted to contact the side chain of Trp-212 of the catalytic loop. A corresponding methyl group is present in the substrate 1-deoxyxylulose 5-phosphate, which supports the view that fosmidomycin actually binds substrate-like and does not represent an analogue of the proposed intermediate 2-*C*-methyl-erythrose 4-phosphate as postulated previously (27). The present model immediately reveals potential interaction sites for specific inhibitors. The pronounced cavity behind the bound fosmidomycin (Fig. 4) can be utilized for stacking interactions with His-257. It should be noted that this cavity is mainly formed by two sequence stretches, His-251 to Ser-258 (His-Pro-Gln-Ser-Leu-Ile-His-Ser) and Pro274 to Arg-277 (Pro-Asp-Met-Arg), which represent highly conserved residues in all available IspC sequences. It additionally harbors the His-251 three water molecules that may be replaced by hydrophilic groups. These are found next to the carbonyl of His-251 and Ile-256, respectively. Substitution at the 3 and 5 positions of the five-member skeleton appear especially suited to include these contacts.

Active Site Geometry and Enzyme Mechanism—Previous structural studies on IspC revealed its principal domain organization (27) and the binding site for NADPH and indicated a phosphate binding site (28). However, no information was available on the binding site for divalent metal ions and the substrate DXP, and no model could be derived for the course of the reaction. The complex of IspC with Mn^{2+} and fosmidomycin now provides a model for the binding mode of the substrate. DXP can be fitted nicely onto fosmidomycin (Fig. 5*a*). During the reaction, the C-4 atom migrates to the C-2 carbon atom, which is partially positively charged because of the polarizing effect of the divalent metal ion. The C-3 hydroxyl is likewise fixed by coordination to the metal ion. This first step is similar to that catalyzed by acetohydroxy acid isomeroreductase, which is involved in the biosynthesis of branched amino acids. There, a carbonyl group is also further polarized by a Mg^{2+} ion, inducing a partial positive charge on the carbon atom (reviewed in Ref. 40).

From stereochemical considerations is has been deduced that the migrating group and the reducing cofactors are located on opposite faces of the planes defined by the metal coordinated α-hydroxycarbonyl substructures (20). A binding mode of the intermediate 2-*C*-methyl-erythrose 4-phosphate (8) in an extended conformation similar to fosmidomycin (9) is not compatible with the stereochemistry of the reduction reaction, as it would result in a hydride transfer to the H_{si} position at C-1 of the product from H_{si} at C-4 of the cofactor and not to H_{re} as observed (20–22). Therefore, we postulate that the putative intermediate does not relax to an extended substrate-like conformation. It is reasonable to assume that the phosphate group of the substrate remains essentially anchored in the phosphate binding site during the reaction. Notably, 1-D-deoxyxylulose does not act as a substrate for the enzyme (19). Therefore, migration of the C-4 atom to the C-2 carbonyl during isomerization will likely require a movement of C-2 toward the phosphate binding site. If it is additionally assumed that the oxygen ligands remain bound to the divalent metal ion throughout the reaction, a binding mode of the intermediate as illustrated in Fig. 5*b* can be modeled.

The NADP-bound IspC model (28) can be superimposed onto our fosmidomycin complex with only minor differences. This allows modeling of NADPH in a substrate complex (Figs. 2 and 5*b*). It should be particularly noted that the resulting geometry of the reaction intermediate not only brings the aldehyde group of the intermediate in close proximity (~ 3.2 Å) to the C-4 position of the NADPH nicotinamide moiety, but also results in the observed hydride transfer to the H_{re} position at C-1 of the product. The methyl group at C-2 is predicted to remain exposed to Trp-212 of the catalytic loop. It has been shown that this methyl group is essential for the affinity of the aldehyde intermediate to the enzyme as D-erythrose 4-phosphate binds significantly weaker (19). The hydride transfer may occur very rapidly, perhaps concomitantly with the isomerization reaction, which is compatible with the fact that the putative intermediate cannot be isolated or trapped. The presence of NADPH during the reaction is assured by an ordered sequential binding starting with NADPH as demonstrated by kinetic studies (23). The finding that the reversible isomerization step requires the presence of NADP+/NADPH indicates that it helps to define the precise active site geometry, presumably by interacting with the flexible active site loop. The strictly conserved residues Trp-212 and Met-214 represent ideal candidates for a stacking interaction or a hydrophobic contact with the nicotinamide moiety of NADPH. We therefore conclude that the catalytic loop and the nicotinamide moiety of NADPH are simultaneously required for their correct positioning at the active site. A recent NMR study demonstrated the proximity of a methionine and an isoleucine residue to the nicotinamide ring portion of NADPH (41). Potential candidates at the active site are Met-214 or Met-276 and Ile-13 or Ile-218, respectively, which all represent almost strictly conserved residues.

In summary, we could demonstrate the binding mode of fosmidomycin to IspC, which must, for stereochemical reasons, be different from that of the aldehyde intermediate, 2-*C*-methyl-erythrose 4-phosphate, as proposed previously. The detailed knowledge of the interaction mode of fosmidomycin as a promising drug against malaria and lead compound may contribute to the development of more potent inhibitors of this key enzyme.

REFERENCES

1. Frankish, H. (2002) *Lancet* **360,** 1075
2. Trouiller, P., Olliaro, P., Torreele, E., Orbinski, J., Laing, R., and Ford, N. (2002) *Lancet* **359,** 2188–2194
3. Wellems, T. E. (2002) *Science* **298,** 124–126
4. Hyman, R. W., Fung, E., Conway, A., Kurdi, O., Mao, J., Miranda, M., Nakao, B., Rowley, D., Tamaki, T., Wang, F., and Davis, R. W. (2002) *Nature* **419,** 534–537
5. Gardner, M. J., Shallom, S. J., Carlton, J. M., Salzberg, S. L., Nene, V., Shoaibi, A., Ciecko, A., Lynn, J., Rizzo, M., Weaver, B., Jarrahi, B., Brenner, M., Parvizi, B., Tallon, L., Moazzez, A., Granger, D., Fujii, C., Hansen, C., Pederson, J., Feldblyum, T., Peterson, J., Suh, B., Angiuoli, S., Pertea, M., Allen, J., Selengut, J., White, O., Cummings, L. M., Smith, H. O., Adams, M. D., Venter, J. C., Carucci, D. J., Hoffman, S. L., and Fraser, C. M. (2002) *Nature* **419,** 531–534
6. Jomaa, H., Wiesner, J., Sanderbrand, S., Altincicek, B., Weidemeyer, C., Hintz, M., Türbachova, I., Eberl, M., Zeidler, J., Lichtenthaler, H. K., Soldati, D., and Beck, E. (1999) *Science* **285,** 1573–1576
7. Missinou, M. A., Borrmann, S., Schindler, A., Issifou, S., Adegnika, A. A., Matsiegui, P.-B., Binder, R., Lell, B., Wiesner, J., Baranek, T., Jomaa, H., and Kremsner, P. G. (2002) *Lancet* **360,** 1941–1942
8. Rohmer, M., Knani, M., Simonin, P., Sutter, B., and Sahm, H. (1993) *Biochem. J.* **295,** 517–524
9. Broers, S. T. J. (1994) *Über die frühen Stufen der Biosynthese von Isoprenoiden in Escherichia coli*. Ph.D. thesis, Eidgenossiche Technische Hochschule Zürich, Zürich, Switzerland
10. Schwarz, M. K. (1994) *Terpen-Biosythese in Gingko biloba: eine überraschende Geschichte.* Ph.D. thesis, Eidgenossiche Technische Hochschule Zürich, Zürich, Switzerland
11. Eisenreich, W., Schwarz, M., Cartayrade, A., Arigoni, D., Zenk, M. H., and Bacher, A. (1998) *Chem. Biol.* **5,** R221–R233
12. Rohmer, M. (1999) in *Comprehensive Natural Product Chemistry* (Cane, D., ed) Vol. 2, pp. 45–68, Pergamon Press, Oxford
13. Schwarz, M., and Arigoni, D. (1999) in *Comprehensive Natural Product Chemistry* (Cane, D., ed) Vol. 2, pp. 367–399, Pergamon Press, Oxford
14. Vial, H. J. (2000) *Parasitol. Today* **16,** 140–141
15. Takahashi, S., Kuzuyama, T., Watanabe, H., and Seto, H. (1998) *Proc. Natl. Acad. Sci. U. S. A.* **95,** 9879–9884
16. Duvold, T., Bravo, J. M., Pale-Grosdemange, C., and Rohmer, M. (1997) *Tetrahedron Lett.* **38,** 4769–4772
17. Arigoni, D., Sagner, S., Latzel, C., Eisenreich, W., Bacher, A., and Zenk, M. H. (1997) *Proc. Natl. Acad. Sci. U. S. A.* **94,** 10600–10605

18. Eisenreich, W., Menhard, B., Hylands, P. J., Zenk, M. H., and Bacher, A. (1996) *Proc. Natl. Acad. Sci. U. S. A.* **93,** 6431–6436
19. Hoeffler, J.-F., Tritsch, D., Grosdemange-Billiard, C., and Rohmer, M. (2002) *Eur. J. Biochem.* **269,** 4446–4457
20. Arigoni, D., Giner, J.-L., Sagner, S., Wungsintaweekul, J., Zenk, M. H., Kis, K., Bacher, A., and Eisenreich, W. (1999) *Chem. Comm.*, 1027–1028
21. Radykewicz, T., Rohdich, F., Wungsintaweekul, J., Herz, S., Kis, K., Eisenreich, W., Bacher, A., Zenk, M. H., and Arigoni, D. (2000) *FEBS Lett.* **465,** 157–160
22. Proteau, P. J., Woo, Y. H., Williamson, R. T., and Phaosiri, C. (1999) *Org. Lett.* **1,** 921–923
23. Koppisch, A. T., Fox, D. T., Blagg, B. S. J., and Poulter, D. C. (2002) *Biochemistry* **41,** 236–243
24. Eisenreich, W., Rohdich, F., and Bacher, A. (2001) *Trends Plant Sci.* **6,** 78–84
25. Kuzuyama, T., Shimizu, T., Takahashi, S., and Seto, H. (1998) *Tetrahedron Lett.* **39,** 7913–7916
26. Zeidler, J., Schwender, J., Muller, C., Wiesner, J., Weidemeyer, C., Beck, E., Jomaa, H., and Lichtenthaler, H. K. (1998) *Z. Naturforsch.* **53,** 980–986
27. Reuter, K., Sanderbrand, S., Jomaa, H., Wiesner, J., Steinbrecher, I., Beck, E., Hintz, M., Klebe, G., and Stubbs, M. T. (2002) *J. Biol. Chem.* **277,** 5378–5384
28. Yajima, S., Nonaka, T., Kuzuyama, T., Seto, H., and Ohsawa, K. (2002) *J. Biochem.* **131,** 313–317
29. Hecht, S., Wungsintaweekul, J., Rohdich, F., Kis, K., Radykewicz, T., Schuhr, C. A., Eisenreich, W., Richter, G., and Bacher, A. (2001) *J. Org. Chem.* **66,** 7770–7775
30. Otwinowski, Z., and Minow, W. (1997) *Methods Enzymol.* **276,** 307–326
31. Collaborative Computational Project No. 4. (1994) *Acta Crystallogr. Sect. D Biol. Crystallogr.* **50,** 760–763
32. Turk, D. (1992) *Weiterentwicklung eines Programms für Molekülgraphik und Elektronendichte-Manipulation und seine Anwendung auf verschiedene Protein-Strukturaufklärungen.* Ph.D. thesis, Technische Universität München, Munich, Germany
33. Brünger, A. T., Adams, P. D., Clore, G. M., DeLano, W. L., Gros, P., Grosse-Kunstleve, R. W., Jiang, J. S., Kuszewski, J., Nilges, M., Pannu, N. S., Read, R. J., Rice, L. M., Simonson, T., and Warren, G. L. (1998) *Acta Crystallogr. Sect. D Biol. Crystallogr.* **54,** 905–921
34. Laskowski, R. A., MacArthur, M. W., Moss, D. S., and Thornton, J. M. (1993) *J. Appl. Crystallogr.* **26,** 283–291
35. Ramachandran, G. N., and Sasisekharan, V. (1968) *Adv. Protein Chem.* **23,** 283–438
36. Esnouf, R. M. (1997) *J. Mol. Graph.* **15,** 132–134
37. Rowsell, S., Hawtin, P., Minshull, C. A., Jepson, H., Brockbank, S. M. V., Barratt, D. G., Slater, A. M., McPheat, W. L., Waterson, D., Henney, A. M., and Pauptit, R. A. (2002) *J. Mol. Biol.* **319,** 173–181
38. Kuzuyama, T., Takahashi, S., Takagi, M., and Seto, H. (2000) *J. Biol. Chem.* **275,** 19928–19932
39. Okuhara, M., Kuroda, Y., Goto, T., Okamoto, M., Terano, H., Kohsaka, M., Aoki, H., and Imanaka, H. (1980) *J. Antibiot.* **33,** 13–17
40. Dumas, R., Biuo, V., Halgand, F., Douce, R., and Duggleby, R. G. (2001) *Acc. Chem. Res.* **34,** 399–408
41. Pellecchia, M., Meininger, D., Dong, Q., Chang, E., Jack, R., and Sem, D. S. (2002) *J. Biomol. NMR* **22,** 165–173